Int. J. Electrochem. Sci., 7 **(2012)** 725 - 746

International Journal of
ELECTROCHEMICAL
SCIENCE
www.electrochemsci.org

The Catalytic Activity of Ruthenates $ARuO_3$ (A= Ca, Sr or Ba) for the Hydrogen Evolution Reaction in Acidic Medium

Nada F. Atta[*], *Ahmed Galal* , *Shimaa M. Ali*

Department of chemistry, Faculty of science, Cairo University, Postal code 12613, Giza, Egypt
[*]E-mail: nada_fah1@yahoo.com

Received: 20 October 2011 / *Accepted:* 3 December 2011 / *Published:* 1 January 2012

Ruthenate perovskites $ARuO_3$, (A= Ca, Sr or Ba) were prepared by coprecipitation method. The electrocatalytic activity of the prepared perovskites was investigated toward the hydrogen evolution reaction (HER). X-ray diffraction analysis suggested successful incorporation of Ru^{4+} at the Ca^{2+}, Sr^{2+} and Ba^{2+} cations sites confirming the formation of the orthorhombic perovskite phases of $CaRuO_3$ and $SrRuO_3$ and the hexagonal perovskite phase of $BaRuO_3$. The average particle size for the prepared perovskites was 39.0, 42.2 and 101.4 nm for Ca, Sr and $BaRuO_3$, respectively. Scanning electron micrographs showed a well-defined hexagonal crystal structure in case of $BaRuO_3$, while $CaRuO_3$ and $SrRuO_3$ composed of agglomerations of nearly spherical grains. $CaRuO_3$ showed smaller agglomerations and more cavities than $SrRuO_3$. The influence of the type of A-cation on the catalytic activity for HER was studied by Tafel linear polarization. The order of the electrocatalytic activity was $BaRuO_3$>$CaRuO_3$>$SrRuO_3$. This was shown from the values of the exchange current density, -60.7, -13.1 and -884.6 $\mu A.cm^{-2}$ for Ca, Sr and $BaRuO_3$, respectively. This suggested that the A-site metal ion not only has a strong effect on the stability of the whole crystal configuration but also provides the possibility to improve catalyst performance by synergetic interactions with the B-site metal ion. The activation energy, reaction order and reaction mechanism have been investigated using the electrochemical techniques, Tafel linear polarization and impedance**.** Again, the calculated values of the activation energy gave similar trend for catalytic activity; 42.6, 86.3 and 17.7 kJ/mol for Ca, Sr and $BaRuO_3$respectively. Both Tafel and the impedance data showed that the volmer step is the rate determining step. In addition, the effect of the partial substitution at the A-site in $Sr_{1-x}Ca_xRuO_3$ was also studied. The catalytic activity of ternary perovskites was about twice higher than that of binary ones. The catalytic activity of ternary oxides increased with increasing the fraction of Ca-doped.

Keywords: Perovskites, Catalyst, Tafel, Impedance, SEM and XRD.

1. INTRODUCTION

Hydrogen is an ideal fuel due to the advantages of no pollution, high combustion heat and abundant sources. The hydrogen evolution reaction (HER), in particular, is an attractive reaction that

illustrates the importance of research in the field of renewable energy. There is a significant technological interest in this reaction due to its important role in electrodeposition and corrosion of metals in acids, in storage of energy via hydrogen production, and as the microscopic reverse of the hydrogen oxidation reaction in low-temperature fuel cells [1-3]. These applications have motivated a significant amount of research on the HER, from the development of fundamental reactivity theories to the investigation of biomimetic catalysts for the reaction [4-15]. The electrocatalysis in the HER is one of the most important subjects in the field of electrochemistry. The study of this reaction has permitted the development of the fundamentals of the electrode kinetics as well as improving the technology of hydrogen production from water electrolysis. In order to reduce energy consuming of water electrolysis, high catalytic activated cathode materials are urgently needed. Three properties play an important role in selecting catalytically active materials for hydrogen evolution: (a) an actual intrinsic electrocatalytic effect of the material, (b) a large active surface area per unit volume ratio, both of which are directly related to the overpotential used to operate the electrolyser at significant current densities, and (c) catalyst stability. Noble metals such as Pt, Pd, Ru, etc. were used in this field [16-18]. Although Pt and Pd have a high catalytic activity for HER, and Pd has a good capacity for hydrogen storage, their limited reserves in the earth restricts their wide application in industry [19, 20].

The well known reaction steps in acidic solutions are [21]:

$$M + H_3O^+ + e^- \leftrightarrow MH_{ads} + H_2O \quad (1)$$

$$MH_{ads} + H_3O^+ + e^- \leftrightarrow H_2 + M + H_2O \quad (2)$$

$$MH_{ads} + MH_{ads} \leftrightarrow H_2 + 2M \quad (3)$$

HER starts with the proton discharge (Volme reaction, Eq. (1)), and follows either electrodesorption step (Heyrovsky reaction, Eq. (2)), or the proton recombination step, physical desorption, (Tafel reaction, Eq. (3)). The distinction between steps (1), (2) and (3), as the rate controlling, is usually accomplished in terms of Tafel slopes or by calculating the rate constants of the forward and backward reactions through simultaneous fitting of polarization and impedance data. According to the general model for the HER mechanism, if the Volmer reaction is the rate determining step, the resulting Tafel curve should yield a slope of 118 $mV.dec^{-1}$ at 20°C. If Heyrovsky step is rate determining, the measured Tafel slope would yield a value of about 40 $mV.dec^{-1}$, or 30 $mV.dec^{-1}$ for the Tafel desorption step [22].

Ruthenium compounds have been extensively studied due to their catalytic activity for many reactions of commercial and environmental importance [23-27]. However, the volatility of RuO_2 at higher temperatures, especially under oxidative atmosphere, has restricted its applications for high temperature catalytic reactions, including auto-exhaust pollution control. Many attempts have been made to synthesize thermally stable ruthenium compounds in order to stabilize Ru in oxide matrix. Ruthenium based perovskites show relatively much better thermal stability and tailored catalytic properties than RuO_2, which makes them attractive for high temperature catalytic applications. Perovskite-type oxides have the general formula ABO_3 (A: alkaline earth or lanthanide; B: transition

element). A is a large cation, responsible for the thermal resistance, and B is a redox cation, responsible for catalytic activity. When subjected to reduction processes, perovskite-type oxides produce very small particles, in the order of nanometers, with high metallic dispersion [28-29]. The efficient use of these catalyst precursors requires a high dispersion of the metal phase, which can be achieved by controlled segregation of the active phase. $ARuO_3$ (A = Ca, Sr and Ba) compounds crystallize in different structures for different A cation [30]. The structure of $CaRuO_3$ and $SrRuO_3$ is similar to that of rare earth orthoferrites, namely orthorhombic $GdFeO_3$. However rare earth orthoferrites are electrical insulators, whereas $ARuO_3$ compounds are good electrical conductors. Powder X-ray diffraction measurements showed significant orthorhombic distortion in $CaRuO_3$ whereas very little distortion was observed in $SrRuO_3$. These structures are comprised of a three-dimensional network of vertex sharing RuO_6 octahedra with alkaline earth cations occupying 12 coordinate voids in the network. $ARuO_3$ (A = Ca, Sr and Ba) compounds have been known for several decades, their crystal structure is still a controversial issue [31-34]. Earlier crystal structure reports indicate that both $CaRuO_3$ and $SrRuO_3$ are othorhomically distorted $GdFeO_3$ type structure [31, 35], whereas recent investigations assigned cubic lattice for $SrRuO_3$ and orthorhombic for $CaRuO_3$ [34]. $BaRuO_3$ crystallizes in hexagonal perovskite structure consisting of face sharing octahedral [36]. Hexagonal $BaRuO_3$ provides an example of complex oxide structure based on close packed stacking of BaO_3 layers.

In the present work, metal ruthenate perovskites were prepared by coprecipitation method. The influence of the A-cation type in $ARuO_3$ on the surface and catalytic properties in HER was described. In addition the effect of the partial substitution at the A-site, $Sr_{1-x}Ca_xRuO_3$ on the catalytic activity was investigated.

2. EXPERIMENTAL METHODS

2.1. Reagents

Ruthenium chloride hydrate (Fluka, purum;41% Ru), Barium Chloride, Strontium chloride and Calcium chloride dihydrate, Sulfuric acid, Potassium hydroxide (Aldrich), Graphite powder (Sigma-Aldrich, <20 micron, synthetic) and Paraffin oil (Fluka) were used as received without further purification. All solutions were prepared using double distilled water. All measurements were made in oxygen-free solution, which was achieved by continuous purging of the cell electrolyte with nitrogen gas (99.999% pure).

2.2. Electrochemical cell and equipments

A standard three-electrode, one compartment cell was used in all experiments. The counter electrode was a large area platinum electrode. The reference electrode was commercially available saturated silver/silver chloride electrode.

The working electrode was carbon paste electrode CPE (d=0.63cm), the unmodified CPE was prepared as follows: 0.125 g of reagent grade graphite powder was taken, washed with acetone, and dried which was then mixed with 45µL of paraffin oil. To modify the CPE, the graphite powder was mixed with the modifier in a certain composition ratio. Both unmodified and modified carbon pastes were packed into a Teflon holder that had been cut off at the end. Electrical contact to the paste was established via a thin copper rod passed through the Teflon holder. The fresh surfaces were obtained by polishing the electrodes on a clean paper until they showed a smooth and shiny appearance after every measurement.

All electrochemical measurements, the DC polarization and the electro-chemical impedance spectroscopy (EIS), were carried out in aqueous acid 0.1M H_2SO_4 by using a Gamry-750 system and a lock-in-amplifier that are connected to a personal computer.

DC polarization measurements of hydrogen evolution were carried out by first stabilization at open-circuit potential (OCP) until a steady-state OCP value was obtained (usually about 30 min.), then conditioning the electrode at -0.2V for 10 min. and at -0.3V for 5 min. Then a linear polarization measurement was made starting from -0.3V to -0.6V, at a scan rate of $1mV.s^{-1}$. The DC polarization measurement was followed by a set of electrochemical impedance spectroscopy measurements at selected overpotentials.

The order of the reaction with respect to H^+ was determined at constant ionic strength of the solution by varying the H_2SO_4 concentration between 0.05 and 0.5M (6 solutions), keeping the ionic strength constant with Na_2SO_4. Only one DC polarization measurement was taken at each H_2SO_4 concentration by the same procedure mentioned above.

The Scanning electron microscopy analysis was done by using JEOL JSM-6360LA and Philips XL30. While, the X-ray diffraction analysis was obtained using Shimadzu XRD-700.

2.3. Preparation of $ARuO_3$ by coprecipitation

Weighed amounts of $RuCl_3.xH_2O$ and $ACl_2{\cdot}2H_2O$, (A = Ca, Sr or Ba) were dissolved in distilled water and stirred for 5 min. with a magnet stirrer. 3M aqueous KOH solution was added with stirring until the pH of the reaction medium reached 13, a black precipitate immediately formed. The solution was kept stirred for 1 h. at room temperature, then allowed to stand for several hours, and washed with distilled water several times in order to remove potassium ion. Then the precipitate was filtrated, dried in an oven at 70°C, ground in a mortar for 10 min. and finally calcinated at 600, 800, and 900ºC in a muffle furnace for 5 h. for obtaining nano-crystalline $SrRuO_3$, $CaRuO_3$, and $BaRuO_3$ respectively.

2.4. Preparation of $Sr_{1-x}Ca_x\ RuO_3$ by coprecipitation

According to the nominal formula of perovskite $Sr_{1-x}Ca_x\ RuO_3$ (x=0, 0.25, 0.5, 0.75 and 1), a series of catalysts was prepared by coprecipitation method as mentioned above.

3. RESULTS AND DISCUSSION

3.1. XRD and surface characterization

$ARuO_3$ (A = Ca, Sr and Ba) perovskites were prepared by coprecipitation method. The prepared compositions were characterized by X-ray powder diffractograms.

Figure 1 shows the XRD of (A) $CaRuO_3$, (B) $SrRuO_3$, (C) $BaRuO_3$ prepared by coprecipitation method. The major diffraction peaks of the as-synthesized powders were matched with the theoretical ones. $CaRuO_3$ showed the broadest diffraction profile than $SrRuO_3$ and $BaRuO_3$ due to formation of the smallest particle, this was expected since the ionic radii of A cation increases from Ca (1.34Å), Sr (1.44 Å) to Ba (1.61 Å).

Thus Ba compounds have largest unit cell dimensions compared to Ca and Sr compounds, this will be confirmed later by SEM.

The results showed successful incorporation of Ru^{4+} at the Ca^{2+}, Sr^{2+} and Ba^{2+} cations sites confirming the formation of the orthorhombic perovskite phases of $CaRuO_3$ and $SrRuO_3$ and the hexagonal perovskite phase of $BaRuO_3$.

In addition to the phase identification, some important structural parameters were calculated from XRD data such as, particle size, lattice parameters, lattice volume and theoretical density [37]. The particle size was calculated from Scherrer equation:

$$\tau = K \lambda / \beta \cos\theta \qquad (4)$$

where τ is the mean crystallite dimension, K is the shape factor, λ is the x-ray wavelength, typically 1.54 Å, β is the line broadening at half the maximum intensity (FWHM) in radians, and θ is the Bragg angle.

The dimensionless shape factor has a typical value of about 0.9, but varies with the actual shape of the crystallite. The Scherrer equation is limited to nano-scale particles. It is not applicable to grains larger than about 0.1 μm.

In case of orthorhombic crystal structure, the lattice parameters a, b, and c are related to the d value through the equation:

$$1/d^2 = h^2/a^2 + k^2/b^2 + l^2/c^2 \quad (5)$$

The lattice volume is given by:

$$V = abc \qquad (6)$$

And for the hexagonal crystal structure the lattice parameters a and c are related to the d value though the equation:

$$1/d^2 = 4/3\ (h^2 + hk + k^2) / a^2 + l^2 / c^2 \qquad (7)$$

And the lattice volume is given by:

$$V = 0.866a^2c \qquad (8)$$

Finally, the theoretical density equals to:

$$D_{theo} = Z\ M / N_A\ V \qquad (9)$$

where, Z is a parameter related to the crystal structure, M is the molecular weight of the sample, N_A is Avogadro's number and V is the lattice volume.

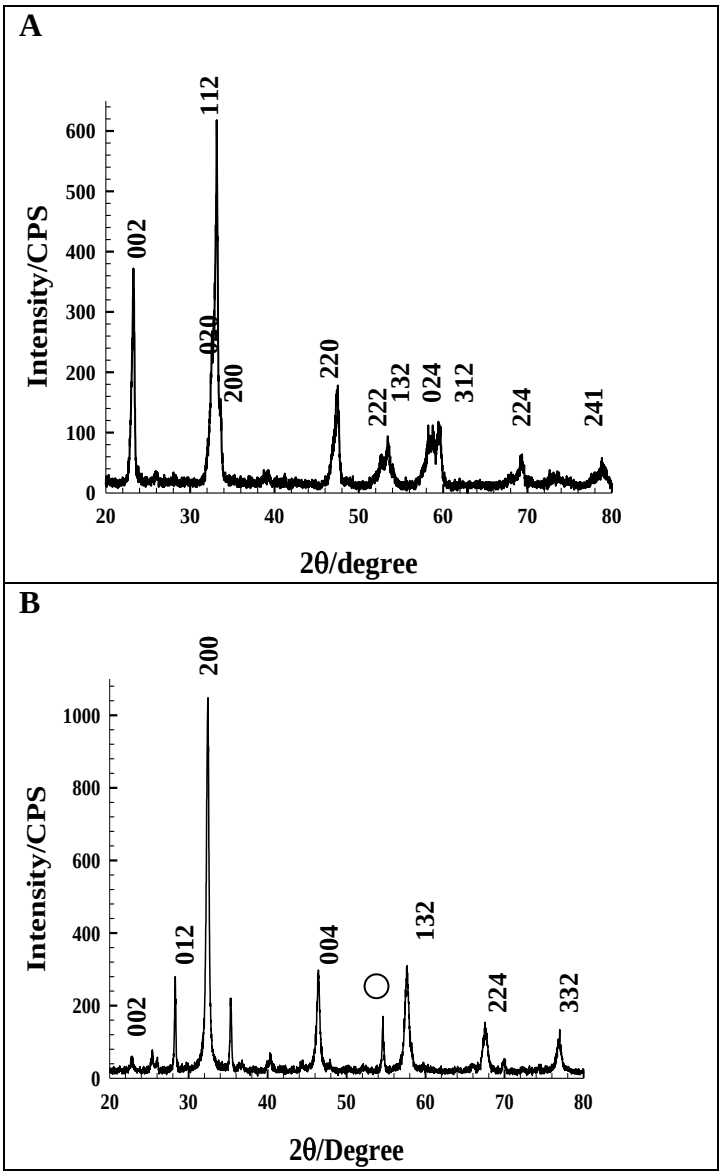

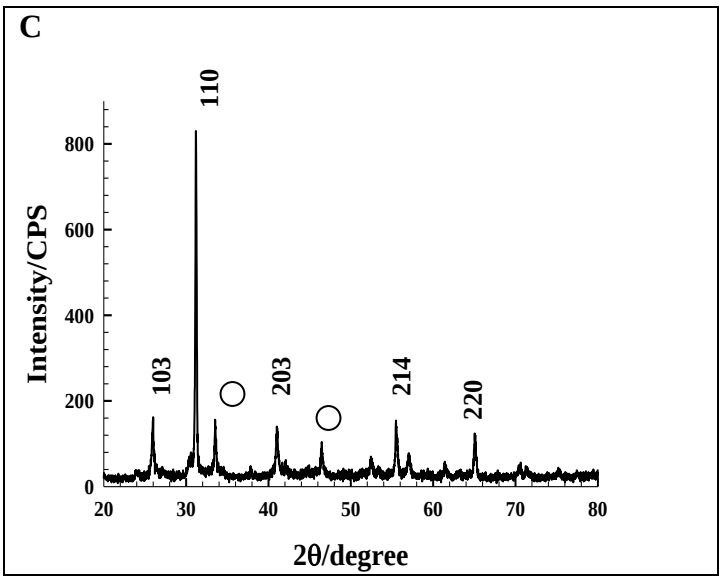

Figure 1. XRD patterns of (A) $CaRuO_3$, (B) $SrRuO_3$ and (C) $BaRuO_3$ prepared by coprecipitation method, (○ Secondary phase, RuO_2). Miller indices (h, l, k) are showed.

The calculated structural parameters from XRD data were listed in Table 1.

Table 1. Structural parameters calculated from XRD data for $ARuO_3$ prepared by coprecipitation method.

	Crystal Structure	Average Partical Size/nm	Lattice Parameters Å	Lattice Volume Å^3	Theoretical density g/cm^3
$CaRuO_3$ Standard	Orthorhombic		a = 5.36 b = 5.54 c = 7.67	227.85	5.51
$CaRuO_3$ Coprecipitation	Orthorhombic	38.99	a = 5.38 b = 5.48 c = 7.67	226.22	5.55
$SrRuO_3$ Standard	Orthorhombic		a = 5.56 b = 5.55 c = 7.86	242.54	6.48
$SrRuO_3$ Coprecipitation	Orthorhombic	42.17	a = 5.71 b = 5.42 c = 7.77	240.38	6.54
$BaRuO_3$ Standard	Hexagonal		a = 5.73 c =14.07	399.37	7.15
$BaRuO_3$ Coprecipitation	Hexagonal	101.43	a = 5.73 c =14.11	401.39	7.11

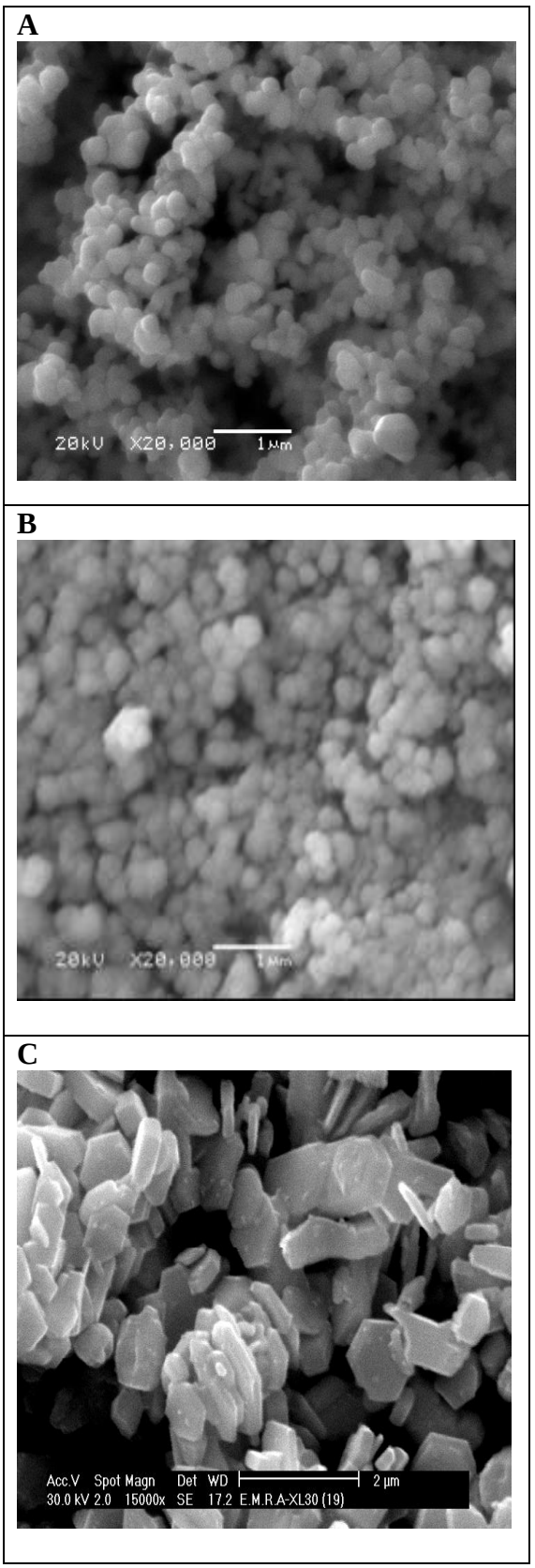

Figure 2. SEM micrographs of (A) $CaRuO_3$, (B) $SrRuO_3$ with a magnification of 20,000 times and (c) $BaRuO_3$ with a magnification of 15,000 times, prepared by coprecipitation method.

These parameters were found to be in good agreement with those for standards. It can be concluded that changing the A cation in $ARuO_3$ affected both the morphology and the particle size of the prepared perovskites.

The morphology was also studied by SEM. Figure 2 shows the SEM images of (A) $CaRuO_3$, (B) $SrRuO_3$ and (C) $BaRuO_3$ prepared by coprecipitation method.

A well-defined hexagonal crystal structure was showed in case of $BaRuO_3$, while $CaRuO_3$ and $SrRuO_3$ composed of agglomerations of nearly spherical grains. $CaRuO_3$ showed smaller agglomerations and more cavities than $SrRuO_3$. Again, changing the A-cation in $ARuO_3$ affected both the morphology and the particle size of the prepared perovskites.

3.2. Investigation of the catalytic activity toward HER by DC-Tafel linear polarization

The electrocatalytic activity of the prepared perovskites, $ARuO_3$ (A = Ca, Sr and Ba), toward HER was investigated by Tafel linear polarization measurements. Figure 3 shows a set of Tafel curves recorded in 0.1 M H_2SO_4 in the potential region of hydrogen evolution for carbon paste electrodes modified with 10% (w/w%) $ARuO_3$ (A = Ca, Sr and Ba) prepared by coprecipitation method.

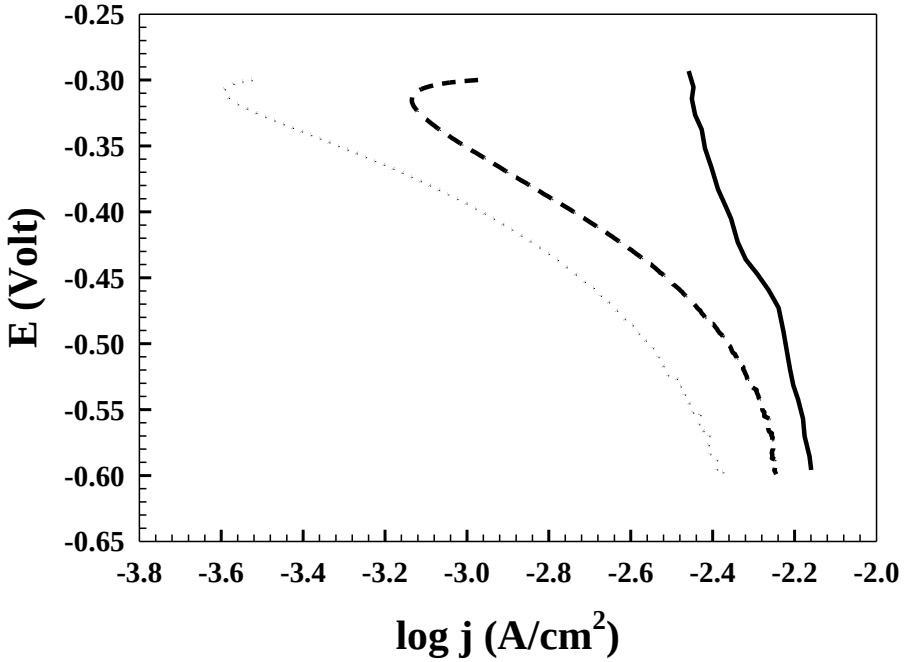

Figure 3. Linear Tafel polarization curves for the HER recorded on CPEs modified with 10% (w/w%) (---) $CaRuO_3$, (…) $SrRuO_3$ and (—) $BaRuO_3$ prepared by coprecipitation method in 0.1M H_2SO_4, scan rate=1 $mV.s^{-1}$.

At low overpotentials, the curves were characterized by a well-defined Tafelian behavior, while at higher overpotentials, a significant deviation from Tafelian behavior was recorded. The existence of two Tafel regions (change in Tafel slope) has already been reported in literature [38] for similar HER electrocatalytic materials, and a number of explanations have been given, a change in HER mechanism

has been suggested as one possible explanation, which can be attributed to the depletion of the d-electron density at the Fermi level of the perovskite by adsorbed hydrogen [39] which remained partially uncompensated at lower ovepotentials. Mass-transport limitations through narrow pores on the catalyst surface [40] or a decrease in the active surface area [41-43] have also been suggested as possible reason for the observed diffusion-like shape of the Tafel curves.

By considering the Tafelian region, it is clearly that the HER on carbon paste electrode modified with these catalysts was kinetically controlled reaction described by the Tafel equation:

$$\eta = a + b \log j \qquad (10)$$

where, η (V) represents the applied overpotential, j ($A.cm^{-2}$) the measured current density, b ($V.decade^{-1}$) the Tafel slope which equals $-2.3RT/\beta nF$ and a (V) is the intercept which related to the exchange current density j_o ($A.cm^{-2}$) through the equation:

$$a = 2.3RT \log j_o/\beta nF \qquad (11)$$

where, n represents the number of electrons exchanged, F = 96,485 ($C.mol^{-1}$) is Faraday constant, R = 8.314 ($J.mol^{-1}.K^{-1}$) is the gas constant, T (K) is the temperature and β is the symmetry factor. The values of Tafel slope, exchange current density, and transfer coefficient calculated for $ARuO_3$ (A = Ca, Sr and Ba) compounds prepared by coprecipitation method were calculated and listed in Table 2 (insert Table 2). According to the general HER mechanism in acidic media [44-46], these Tafel slope values indicated that the Volmer reaction step i.e. adsorption of hydrogen on the catalyst was the rate-determining step. It could also be noticed that the Tafel slope and transfer coefficient values deviated from the theoretical values 116 mV $decade^{-1}$ and 0.5 respectively [44-46]. This phenomenon has already been reported in the literature [44] and has been explained as a characteristic feature for oxide catalysts. Note that for the Volmer step the symmetry factor, β, is equal to the transfer coefficient, α, while for the Heyrovsky step, i.e. desorption of adsorbed hydrogen to form molecular hydrogen, the transfer coefficient α is equal $1+\beta$ [44-46]. Considering the exchange density values, presented in Table 3 one can conclude that the order of the electrocatalytic activity is $BaRuO_3 > CaRuO_3 > SrRuO_3$. However, although a value of exchange current density is frequently used for the characterization of electrocatalytic activity, it has been reported that values of Tafel slope and transfer coefficient in the low overpotential region (Tafelian region) were as or even more important than a favorable exchange current density value [47]. This is due to the fact that the HER does not occur at a reversible potential (i.e. zero overpotential), but a certain overpotential is required for the reaction to proceed at a measurable rate. Hence, in order to compare the electrocatalytic activity of the catalysts prepared by different methods at the conditions relevant for the operation of hydrogen generator, one can fix current density (i.e. hydrogen production rate) and compare the resulting overpotentials required to reach the given current density value. This would give an indication on the amount of energy (overpotential) that should be invested to produce a specified amount of hydrogen (since the current is, through the Faraday law, directly related to the amount of the produced

hydrogen). Overpotential values for each catalyst, measured at current density of 1 $mA.cm^{-2}$, were presented in Table 2.

Table 2. HER kinetics parameters (the Tafel slope, exchange current density, transfer coefficient, overpotential measured at a current density of 1 mA cm^{-2} and current density at a fixed overpotential of -300mV) obtained by analysis of Linear Tafel polarization curves for for $ARuO_3$ prepared by coprecipitation method.

Catalyst	b/mV.dec^{-1}	j_0/μA.cm^{-2}	α	j/μA.cm^{-2} at -300mV	η /mV at 1mA/cm^{-2}
$CaRuO_3$	277.8	-60.7	0.212	-1064.9	-352.0
$SrRuO_3$	219.5	-13.1	0.269	-298.0	-394.0
$BaRuO_3$	807.1	-884.6	0.073	-3687.2	-81.4

Another common way of comparing the electrocatalytic activity of HER electrocatalysts is to fix the overpotential (energy input) and then compares the resulting current density values, i.e. the amount of hydrogen that would be produced by each catalyst. The results for overpotential of -300mV were presented in Table 2. By considering both the current density values, measured at a fixed overpotential of -300mV and the overpotential values, measured at current density of 1 $mA.cm^{-2}$, presented in Table 2, similar trend was observed and the same order of the electrocatalytic activity was found. This trend can be explained on the basis that $CaRuO_3$ has a higher catalytic activity toward HER than $SrRuO_3$ as a consequence of the increasing its surface area which can be clearly shown from the SEM pictures presented in Figure 2. However, the surface area can not be taken as the only factor controlling the electrocatalytic activity and this is clear since $BaRuO_3$, which has the smallest surface area among $ARuO_3$ compounds, has the highest electrocatalytic activity. Another factor affecting the catalytic activity and is even much more important is the type of A-site metal ion (in the ABO_3-type perovskite) [48], where A-site metal ion not only has a strong effect on the stability of the whole crystal configuration but also provides the possibility to improve catalyst performance by synergetic interactions with the B-site metal ion. In addition, the Ru-Ru bond length in $BaRuO_3$ is much less compared to that in (Ca, Sr)RuO_3 [49] which indicates a strong Ru-Ru bonding in $BaRuO_3$. This strong interaction was also contributing to the highest electrocatalytic activity toward HER observed for $BaRuO_3$.

3.3. Order of reaction with respect to H^+

The order of the reaction with respect to H^+ was determined at constant ionic strength of the solution. Tafel experiments were carried out in x M H_2SO_4 (x = 0.05, 0.1, 0.2, 0.3, 0.4, and 0.5M) in the potential region of hydrogen evolution for carbon paste electrodes modified with 10% (w/w%) $CaRuO_3$, $SrRuO_3$ and $BaRuO_3$ prepared by coprecipitation method, respectively. Figure 4 represents the dependence of the cathodic current of HER on the H^+ ion concentration.

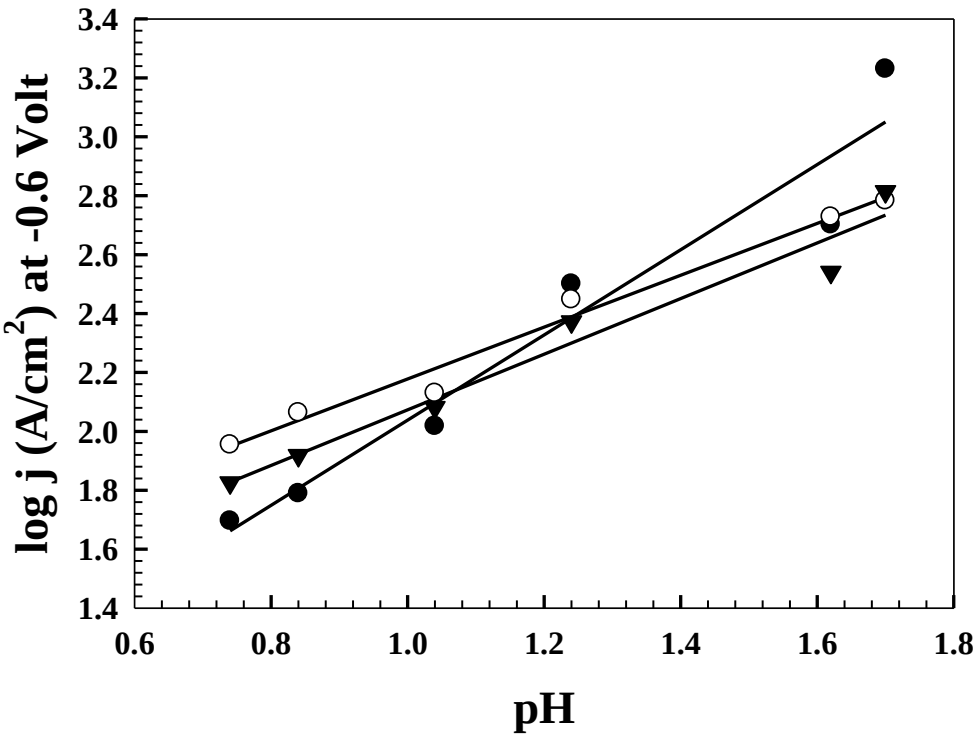

Figure 4. Typical plots of log j (A/cm^2) at -0.6 Volt (Saturated Ag/AgCl) vs. pH for $CaRuO_3$ (▼), $SrRuO_3$ (○) and $BaRuO_3$ (●) prepared by coprecipitation method.

The reaction order values of $ARuO_3$ (A = Ca, Sr and Ba) prepared by coprecipitation were 0.94, 0.88, and 1.03 respectively. The fractional reaction order was expected for HER catalyzed by oxide catalysts [50].

3.4. Activation energy

In order to evaluate the temperature effect on the kinetics of the HER for the prepared catalysts, DC linear polarization (Tafel) measurements were done for a wide temperature range, from 298K to 338K. Figures 5A, 5B and 5C show a set of Tafel curves recorded on carbon paste electrodes modified with 10% (w/w%) $CaRuO_3$, $SrRuO_3$ and $BaRuO_3$ prepared by coprecipitation method respectively, at various temperatures. Figures 5A', 5B' and 5C' demonstrated that this increase was linear in a semi-logarithmic plot, the Arrhenius equation:

$$\log j_o = -2.303E_a/RT + \log A \qquad (12)$$

where, A (A.cm^{-2}) is the pre-exponential factor and E_a (J.mol^{-1}) is the apparent activation energy. Thus, from the slope of the line, the apparent activation energy value could be calculated. The activation energy values for $CaRuO_3$, $SrRuO_3$ and $BaRuO_3$ prepared by coprecipitation method were 42.60, 86.32 and 17.68 kJ.mol^{-1}, respectively.

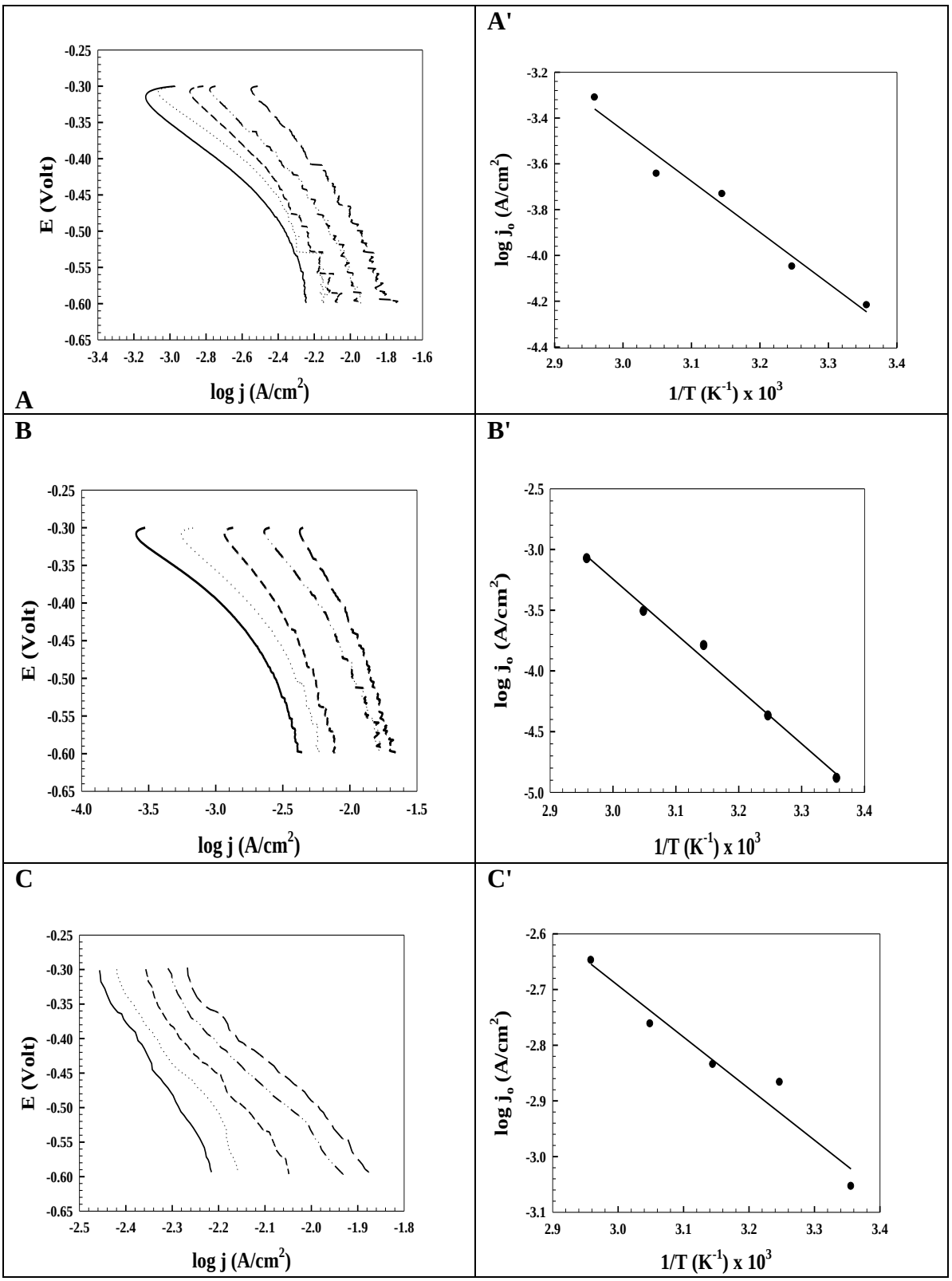

Figure 5. Linear Tafel polarization curves for the HER recorded on CPEs modified with 10% (w/w%) (A) $CaRuO_3$, (B) $SrRuO_3$ and (C) $BaRuO_3$ prepared by coprecipitation method in 0.1M H_2SO_4 at various temperatures; 298 (——), 308 (…), 318 (---), 328 (-..-..-), and 338 K (— —), scan rate=1 $mV.s^{-1}$. And Arrhenius plots for the determination of activation energy values for (A') $CaRuO_3$ and (B') $BaRuO_3$ prepared by coprecipitation method.

Again, this trend agreed well with the trend concluded from Tafel measurements, that is to say, the order of the electrocatalytic activity is $BaRuO_3$>$CaRuO_3$>$SrRuO_3$. The corresponding electrochemical parameters Tafel slopes and transfer coefficients together with the exchange current densities at various temperatures are showed in Table 3.

Table 3. HER kinetics parameters (the Tafel slope, exchange current density and transfer coefficient) obtained by analysis of Linear Tafel polarization curves at various temperatures for $ARuO_3$ prepared by coprecipitation method.

T/K	$CaRuO_3$			$SrRuO_3$			$BaRuO_3$		
	b/mV.dec^{-1}	j_o/μA.cm^{-2}	α	b/mV.dec^{-1}	j_o/μA.cm^{-2}	α	b/mV.dec^{-1}	j_o/μA.cm^{-2}	α
298	277.8	-60.7	0.212	219.5	-13.1	0.269	807.1	-884.6	0.073
308	289.7	-89.5	0.210	257.9	-42.6	0.236	764.7	-1360.5	0.080
318	317.7	-185.7	0.198	334.2	-161.8	0.188	713.0	-1464.6	0.088
328	331.6	-227.8	0.196	326.9	-309.5	0.199	678.2	-1732.1	0.096
338	375.9	-490.1	0.178	410.2	-840.8	0.163	686.8	-2252.1	0.097

The Tafel slope is usually considered to increase proportionally with temperature according to the relation b = RT/αF based on the assumption of a temperature-independent transfer coefficient α [51]. However, in this work, the Tafel slope-temperature relations did not show the expected behavior exactly and a more complicated relation between the Tafel slope and temperature should be considered. According to Conway for electrochemical reactions including the HER on different electrode materials, the transfer coefficient α is supposed to vary linearly with temperature:

$$\alpha = \alpha_H + \alpha_S T \qquad (13)$$

where, α_H and α_S are enthalpy and entropy components [51]. It can be shown that the transfer coefficient for HER on carbon paste electrodes modified with $CaRuO_3$ and $SrRuO_3$ prepared coprecipitation method decreased with temperature. While, it increased with temperature in case of carbon paste electrode modified with $BaRuO_3$, prepared by coprecipitation method. The values of α_H and α_S obtained for the prepared catalysts on the basis of equation (13) were (0.49, 1.00 and -0.12) and (-8.33X10^{-4}, -2.44X10^{-3} and -6.46X10^{-4}) K^{-1} for $CaRuO_3$, $SrRuO_3$ and $BaRuO_3$, respectively.

3.5. Electrochemical impedance spectroscopy:

To ensure a complete characterization of the electrode/electrolyte interface and corresponding processes, EIS measurements were made over a frequency range from 100 KHz to 10 mHz at selected overpotentials from the DC polarization curves. Figures 6A, 6B and 6C show examples of EIS spectra recorded on carbon paste electrode modified with 10% (w/w%) $CaRuO_3$, $SrRuO_3$ and $BaRuO_3$ prepared by coprecipitation method, respectively at different overpotentials.

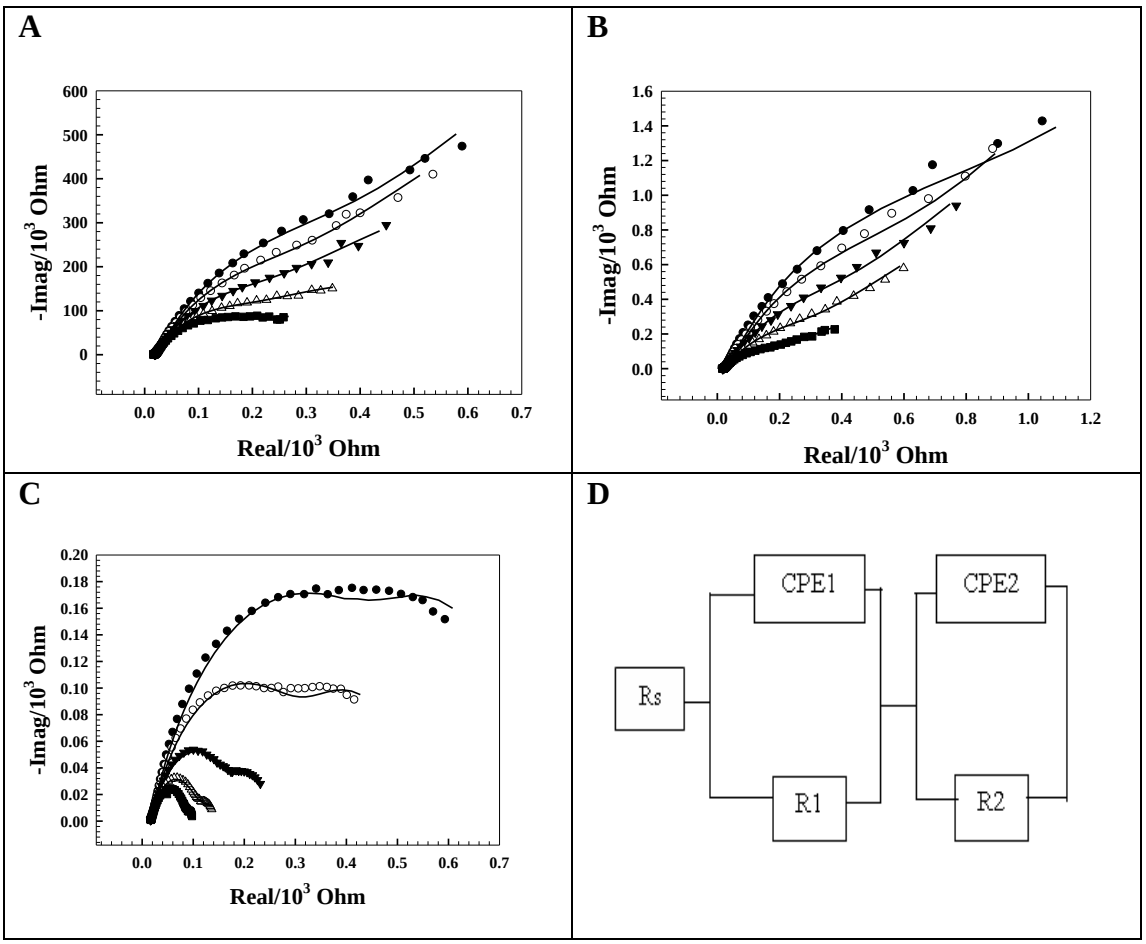

Figure 6. Nyquist plots showing An EIS response of CPEs modified with 10% (w/w%) (A) $CaRuO_3$, (B) $SrRuO_3$ and (C) $BaRuO_3$ prepared by coprecipitation method in 0.1M H_2SO_4 at various ovepotentials, (●) -50, (○) -75, (▼) -100, (Δ) -125 and (■) -150 mV, symbols are experimental and solid lines are modeled data. (D) Electrical equivalent circuit used to explain the EIS response.

The EIS spectra revealed the presence of two time constants. In order to derive a physical picture of the electrode/electrolyte interface and the processes occurring at the electrode surface, experimental EIS data were modeled using non-linear least-squares fit analysis (NLLS) software and electrical equivalent circuit. Figures 6A, 6B and 6C show that a very good agreement between the experimental (symbols) and simulated (lines) data was obtained when the equivalent circuit shown in Figure 6D was used to describe the EIS response of the investigated catalysts. This model has been used o describe the response of the HER on porous electrodes [53-54]. It reflects the response of a HER system characterized by two time constants, only one of them (CPE1) is related to the kinetics of the HER. This time constant changes with overpotential. The second time constant (CPE2) is related to the porosity of the electrode surface, and does not change with overpotential. Tables 4a, 4b, and 4c show the electrical equivalent circuit parameters calculated from NLLS analysis for $CaRuO_3$, $SrRuO_3$ and $BaRuO_3$ prepared by coprecipitation method, respectively.

Table 4. The electrical equivalent circuit parameters calculated from the NLLS analysis for (a) $CaRuO_3$, (b) $SrRuO_3$ and (c) $BaRuO_3$ prepared by coprecipitation.

Table 4a

η/V	Rs/ Ω cm^2	CPE1/F cm^{-2}	m	R1/ Ω cm^2	CPE2/F cm^{-2}	n	R2/ Ω cm^2
-0.050	19.20	476.74	0.61	9341.65	726.25	0.96	208.88
-0.075	19.09	440.47	0.60	4105.98	730.70	0.94	153.71
-0.100	18.91	374.40	0.58	1778.79	763.82	0.92	123.06
-0.125	18.82	315.95	0.56	677.17	815.68	0.91	100.96
-0.150	16.87	203.77	0.49	419.32	885.17	0.89	104.88

Table 4b

η/V	Rs/ Ω cm^2	CPE1/F cm^{-2}	m	R1/ Ω cm^2	CPE2/F cm^{-2}	N	R2/ Ω cm^2
-0.050	18.28	986.17	0.70	1.41×10^9	761.39	1.11	539.16
-0.075	18.08	992.97	0.69	1.59×10^6	607.57	1.13	271.69
-0.100	17.89	844.89	0.66	35841.18	594.82	1.10	158.00
-0.125	17.98	583.67	0.60	18132.33	711.60	1.01	129.01
-0.150	17.85	340.89	0.53	2324.12	621.62	0.96	88.81

Table 4c

η/V	Rs/ Ω cm^2	CPE1/F cm^{-2}	m	R1/ Ω cm^2	CPE2/F cm^{-2}	n	R2/ Ω cm^2
-0.050	17.10	3146.10	0.69	506.02	162.14	0.80	370.70
-0.075	16.91	3143.52	0.67	321.81	147.34	0.84	194.97
-0.100	16.70	3426.15	0.67	175.65	81.13	0.92	58.22
-0.125	15.25	6740.74	0.79	70.70	108.26	0.33	85.01
-0.150	15.42	8492.99	0.77	59.91	42.73	0.26	49.47

With an increase in overpotential, CPE1 changed (decreased in case of $CaRuO_3$ and $SrRuO_3$ and increased in case of $BaRuO_3$) and R1 decreased. It can be concluded that the (CPE1-R1) was related to the HER charge-transfer kinetics, namely to the response of double layer capacitance characterized by CPE1 and HER charge transfer resistance characterized by R1. Contrary to the behavior of CPE1, the value of CPE2 was shown to be relatively constant. At the same time, the value of R2 decreased. This was a typical behavior related to the porosity of the electrode surface.

This EIS behavior is quite in consistence with the Tafel behavior discussed previously. As from the Tafel measurements, the slow rate-determining step in the HER on the carbon paste electrodes modified with perovskites was the adsorption of hydrogen (Volmer), while the desorption step was fast. Consequently, the absence of an EIS hydrogen adsorption time constant could be expected, as also confirmed by the EIS measurements. This demonstrates that although EIS and Tafel techniques are two quite different experimental techniques, results obtained by both techniques are comparable.

3.6. The effect of the partial substitution at the A-site, $Sr_{1-x}Ca_x RuO_3$, on the catalytic activity

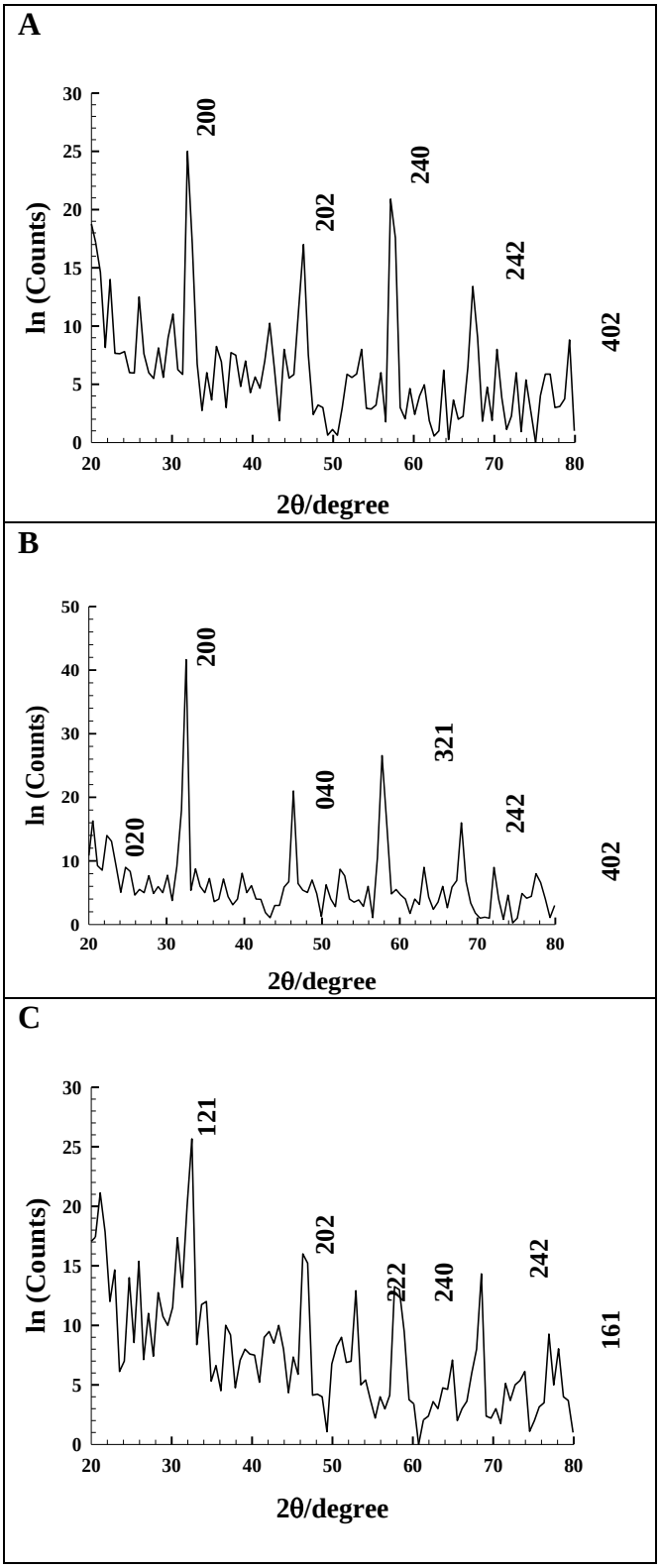

Figure 7. XRD patterns of (A) $Sr_{0.75}Ca_{0.25}RuO_3$, (B) $Sr_{0.5}Ca_{0.5}RuO_3$ and (C) $Sr_{0.25}Ca_{0.75}RuO_3$ prepared by coprecipitation method. Miller indices (h, l, k) are showed.

A series of perovskite catalysts, $Sr_{1-x}Ca_x\ RuO_3$ (x=0, 0.25, 0.5, 0.75 and 1) was prepared by coprecipitation method. Figure 7 shows the XRD patterns of the prepared perovskites, the results suggested the successful formation of ternary perovskites.

The identified phases were $Sr_{0.8}Ca_{0.2}RuO_3$, $Sr_{0.5}Ca_{0.5}RuO_3$ and $Sr_{0.3}Ca_{0.7}RuO_3$ for $Sr_{0.75}Ca_{0.25}RuO_3$, $Sr_{0.5}Ca_{0.5}RuO_3$ and $Sr_{0.25}Ca_{0.75}RuO_3$, respectively.

The structural parameters obtained from XRD data were calculated and listed in Table 5 and found to be in good agreement with those for standards. It can be concluded that ternary Sr-Ca-Ru perovskites prepared in different molar ratios of A cations had different particle size and lattice parameters.

Table 5. Structural parameters calculated from XRD data for $Sr_{1-x}Ca_xRuO_3$ prepared by coprecipitation method.

	Average Partical Size/nm	Lattice Parameters Å	Lattice Volume Å^3	Theoretical density g/cm^3
Standard $Sr_{0.8}Ca_{0.2}RuO_3$		a = 5.53 b = 7.82 c = 5.55	239.86	6.29
$Sr_{0.8}Ca_{0.2}RuO_3$ Coprecipitation	17.12	a = 5.54 b = 7.82 c = 5.56	240.88	6.27
Standard $Sr_{0.5}Ca_{0.5}RuO_3$		a =5.51 b = 7.79 c = 5.49	236.00	5.99
$Sr_{0.5}Ca_{0.5}RuO_3$ Coprecipitation	19.82	a = 5.54 b = 7.79 c = 5.50	237.36	5.96
Standard $Sr_{0.3}Ca_{0.7}RuO_3$		a =5.51 b = 7.74 c = 5.44	232.28	5.82
$Sr_{0.3}Ca_{0.7}RuO_3$ Coprecipitation	13.08	a = 5.44 b = 7.74 c = 5.62	236.61	5.71

The morphology of the prepared perovskites was studied by SEM. Figure 8 shows the SEM images of $Sr_{1-x}Ca_x\ RuO_3$, x = (A) 0.25, (B) 0.5 and (C) 0.75, prepared by coprecipitation method. All phases composed of agglomerations of nearly spherical grains.

However smaller grain size was observed in the ternary phases compared to the binary perovskites. Among the ternary perovskites, the grain size decreased with increasing the fraction of the Ca-doped.

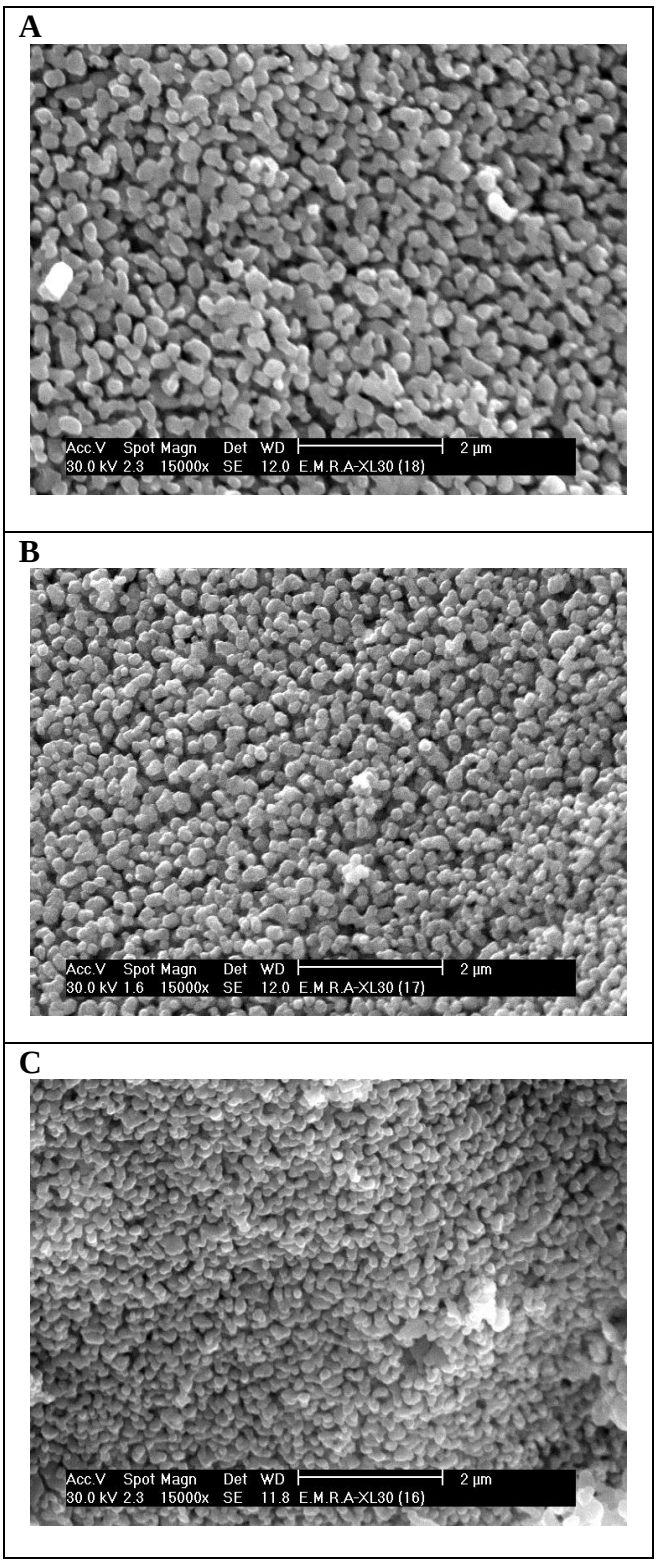

Figure 8. SEM micrographs of (A) $Sr_{0.75}Ca_{0.25}RuO_3$, (B) $Sr_{0.5}Ca_{0.5}RuO_3$ and (C) $Sr_{0.25}Ca_{0.75}RuO_3$ with a magnification of 15,000 times, prepared by coprecipitation method.

The prepared perovskites were tested as catalysts for the HER. Figure 9 shows the dependence of the cathodic current on the faction of Ca in Ca-doped $SrRuO_3$.

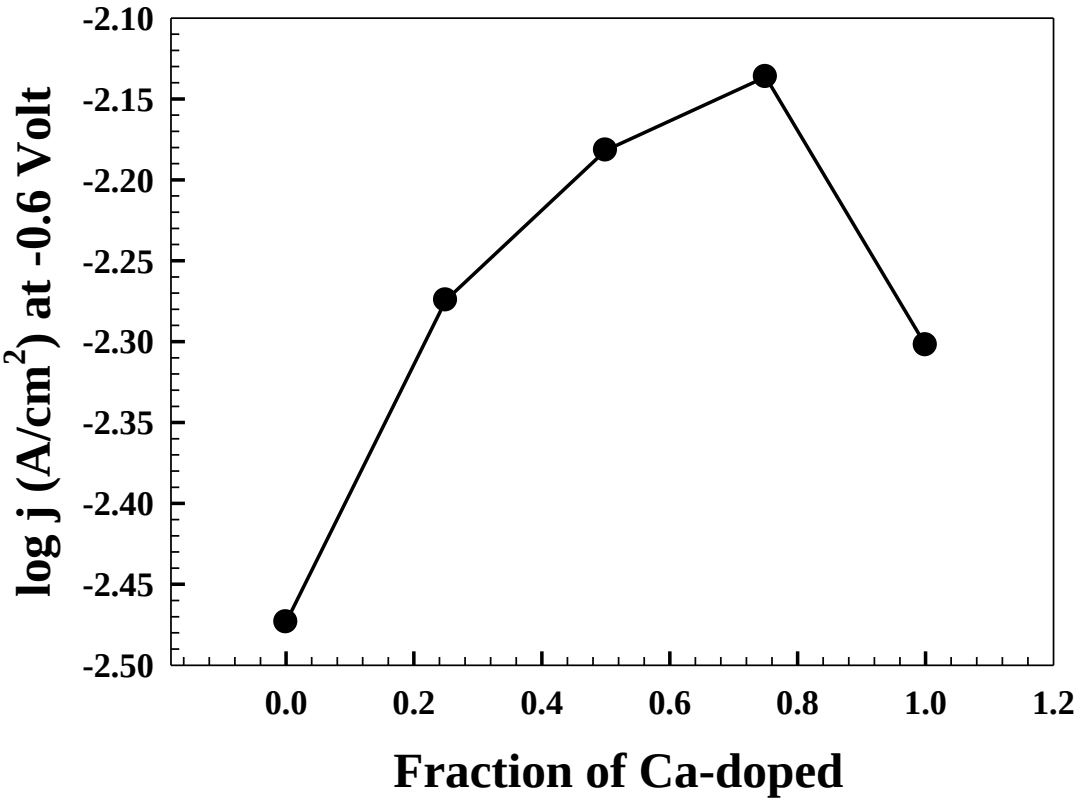

Figure 9. Typical plot of log j (A/cm^2) at -0.6 Volt (Saturated Ag/AgCl) vs. the fraction of Ca-doped.

It is clearly that the presence of two kinds of metal ions in A-site ($Sr_{0.75}Ca_{0.25}RuO_3$, $Sr_{0.5}Ca_{0.5}RuO_3$ and $Sr_{0.25}Ca_{0.75}RuO_3$) enhanced the catalytic activity compared to only one kind A-site metal ion ($SrRuO_3$ and $CaRuO_3$). The reason may be the increased surface area by the presence of two types of metal ions at the A-site compared to the presence of one type, as shown from Figure 8, and the stronger interaction with the B-site metal ion due to the synergetic effect. In case of the two A-site metal ions, the catalytic activity increased by increasing the fraction of Ca-doped. This was because of the increased surface area by increasing the fraction of Ca-doped, as shown by the SEM pictures and also the stronger interaction with the B-site metal ion offered by Ca over Sr increased the stability of the crystal structure [48] and the electrocatalytic activity of perovskites.

4. CONCLUSION

The ruthenates, $ARuO_3$ (A = Ca, Sr or Ba) exhibited a good catalytic activity toward the HER. The order of the electrocatalytic activity was $BaRuO_3 > CaRuO_3 > SrRuO_3$. $BaRuO_3$ has the highest catalytic activity in spite of its largest particle size and smallest surface area compared to $CaRuO_3$, $SrRuO_3$ because of the strongest Ru-Ru bonding in $BaRuO_3$. $CaRuO_3$ has a higher catalytic activity than $SrRuO_3$ not only as a consequence of increasing the surface area but also the stronger affect offered by Ca over Sr as A-site metal ion which not only stabilize the whole crystal configuration but

also provides the possibility to improve catalyst performance by synergetic interactions with the B-site metal ion. The presence of two kinds of metal ions at the A-site, $Sr_{1-x}Ca_xRuO_3$ enhances the catalytic activity compared to only one kind A-site metal ion ($SrRuO_3$ and $CaRuO_3$). In case of two A-site metal ions the catalytic activity increases by increasing the fraction of Ca-doped.

References

1. M.Z. Jacobson, W.G. Colella and D.M. Golden, *Science* 308 (2005) 1901.
2. C.H. Hamann, A. Hamnett and W. Vielstich, Electrochemistry, Wiley-VCH, Weinheim, 1998.
3. CRC Handbook of Chemistry and Physics, CRC Press, New York, 1996.
4. B.E. Conway and J.O.M. Bockris, *J. Chem. Phys*. 26 (1957) 532.
5. R. Parsons, *Trans. Faraday Soc*. 54 (1958) 1053.
6. H. Gerischer, *Bulletin des Societes Chimiques Belges* 67 (1958) 506.
7. S. Trasatti, *Surf. Sci*. 335 (1995) 1.
8. S. Trasatti, *Adv. Electroch. El. Eng*. 10 (1977) 213.
9. L.I. Krishtalik, *Electrokhimiya* 2 (1966) 616.
10. S. Harinipriya and M.V. Sangaranarayanan, *J. Phys. Chem*. B 106 (2002) 8681.
11. J.O.M. Bockris, A.K.N. Reddy and M. Gamboa-Aldeco, Modern Electrochemistry 2A: Fundamentals of Electrodics, Plenum US, New York , 1998.
12. B. Hinnemann, P.G. Moses, J. Bonde, K.P. Jorgensen, J.H. Nielsen, S. Horch, I. Chorkendorff and J.K. Nørskov, *J. Am. Chem. Soc*. 127 (2005) 5308.
13. C. Tard, X.M. Liu, S.K. Ibrahim, M. Bruschi, L.D. Gioia, S.C. Davies, X. Yang, L.S. Wang, G. Sawers and C.J. Pickett, *Nature* 433 (2005) 610.
14. I.G. Medvedev, Russian *J. Electrochem*. 40 (2004) 1123.
15. S. Trasatti, *Electroanal. Chem. Interfacial Electrochem*. 39 (1972) 163.
16. W.K. Hu and J.Y. Lee, *Int. J. Hydrogen Energy* 23 (1998) 253.
17. M.J. Degiz, G. Filho, E.R. Gonzalez and S. Srlnivasan, *Int. J. Hydrogen Energy* 20 (1995) 423.
18. S. Martinez, M. Metiko¡š-Hukovi and L.J. Valek, *Mol. Catal. A-Chem*. 245 (2006) 114.
19. Z. Mme, H. Abdel, J. Pagetti and J. Talbot, *Mater. Chem*. 2 (1977) 83.
20. K. Ashok, Vijh. *Mater. Chem*. 4 (1979) 51.
21. J.M. Jakšić, M.V. Vojnović and N.V. Krstajić, *Electrochim. Acta* 45 (2000) 151.
22. M. Metikoš-Huković, Z. Grubač, N. Radić, A. Tonejc, *Mol. Catal. A-Chem*. 249 (2006) 172.
23. Z. Kowalczyk, S. Jodzis, N. Rarog, J. Zielinski and J. Pielaszek, *Appl. Catal*. A 173 (1998) 153.
24. N.K. Labhsetwar, A. Watanabe, T. Mitsuhashi, SAE Publication No. 2002-28-0044.
25. N.K. Labhsetwar, A. Watanabe, T. Mitsuhashi, SAE Publication No. 2002-01-0019.
26. L. Dahl, K. Jansson and M. Nygren, *Mater. Res. Bull*. 33 (1998) 211.
27. N.K. Labhsetwar, A. Watanabe, T. Mitsuhashi and H. Haneda, *J. Mol. Catal. A Chem*. 223 (2004) 217–223.
28. M.R. Goldwasser, M.E. Rivas, E. Pietri, M.J. Pérez-Zurita, M.L. Cubeiro, A. Griboval-Constant and G. Leclercq, *J. Mol. Catal*. A 228 (2005) 325.
29. G. Valderrama, M.R. Goldwasser, C. Urbina, J.M. Tatibouët, J. Barrault, C. Batiot-Dupeyrat and F. Martínez, *Catal. Today* 107 (2005) 785.
30. M.V. Rama Rao, V.G. Sathe, D. Sornadurai, B. Panigrahi, T. Shripathi, *J. Phys. Chem. Solids* 62 (2001) 797.
31. J.J. Randall, R. Ward, *J. Am. Chem. Soc*. 81 (1959) 2629.
32. R.J. Bouchrad, J.L. Gillson, *Mater. Res. Bull*. 7 (1972) 873.
33. V.I. Spitsyn, I.M. Kulshov, N.F. Shakhova, *Russian J. Inorg. Chem*. 18 (1973) 592.
34. W. Bensch, H.W. Schmalle, A. Reller, *Solid State Ion*. 43 (1990) 171.

35. C.W. Jones, P.D. Battle, P. Lightfoot, W.T.A. Harisson, *Acta Crystallogr.Sec*. C 45 (1989) 365.
36. P.C. Donohue, L. katz, R. Ward, *Inorg. Chem*. 4 (1965) 306.
37. B.D. Cullity, Elements of X-ray diffraction, 2nd ed., addision Wealey pub. company, U.S.A, 1978.
38. A.Damian and S. Omanovic, *J. Power Sources* 158 (2006) 464.
39. K.R. Christmann, In: Z. Poal, P.G. Menon (Eds), Hydrogen Effects in Catalysis, Marcel Dekker, Chapter 1, 1988.
40. J.G. Highfield, K. Oguro, B. Grushko, *Electrochim. Acta* 47 (2001) 465.
41. A.Rami, A. Lasia, *J. Appl. Electrochem*. 22 (1992) 376.
42. N. Krstajic, S. Trasatti, *J. Appl. Electrchem*. 28 (1998) 1291.
43. C.A. Marozzi, A.C. Chialvo, *Electrochim. Acta* 46 (2001) 861.
44. Southampton Electrochemistry group, Instrumental Methods in Electrochemistry, Wiley, New York, 1985.
45. B. Borresen, G. Hagen, R. Tunold, *Electrochim Acta* 47 (2002) 1819.
46. E. Ndzebet, O. Savadogo, *Int. J. Hydrogen Energy* 20 (1995) 635.
47. R. Simpraga, G. Tremiliosi-Filho, S.Y. Qian, B.E. Conway, *J. Electroanal. Chem*. 424 (1997) 141.
48. A.Qi, S. Wang, G. Fu, C. Ni and D. Wu, *Applied catalysis A:General* 281 (2005) 233.
49. M.V. Rama Rao, V.G. Sathe, D. Sornadurai, B. Panigrahi, T. Shripathi, *J. Phys. Chem. Solids* 62 (2001) 797.
50. E. Fachinotti, E. Guerrini, A.C. Tavares and S. Tasatti, *J. Electroanal. Chem*., 600 (2007) 103.
51. B.E. Conway, In: A. Wieckowski, editor. Interfacial electrochemistry. New York: Marcel Dekker, 1999.
52. D.B. Sepa. In: J.O.M. Bockris, B.E. Conway, R.E. White, editor. Modern aspects of electrochemistry, New York: Plenum Press, 1996.
53. B. Losiewicz, A. Budniok, E. Rowinski, E. Lagiewka, A. Lasia, *Int. J. Hydrogen Energy* 29 (2004) 145.
54. L. Birry, A. Lasia, *J. Appl. Electrochem*. 34 (2004) 735.